IIETA International Information and Engineering Technology Association
Advancing the World of Information and Engineering

Journal Européen des Systèmes Automatisés
Vol. 58, No. 2, February, 2025, pp. 271-282
Journal homepage: http://iieta.org/journals/jesa

A Novel Elliptical Savonius Turbine Integrated with Gearless Axial Generator

Sri Kurniati*, Sudirman Syam, Nursalim

Department of Electrical Engineering Faculty of Science and Technology, Nusa Cendana University, Kupang-NTT 85228, Indonesia

Corresponding Author Email: sri_kurniati@staf.undana.ac.id

https://doi.org/10.18280/jesa.580208

Received: 12 January 2025
Revised: 13 February 2025
Accepted: 19 February 2025
Available online: 28 February 2025

Keywords:
wind power, power coefficient, voltage output, AFPM generator, wind turbine, load current, efficiency, end plate

ABSTRACT

This study investigates the performance of an elliptical Savonius turbine integrated with an axial generator that operates a gearless transmission. The turbine's design has been modified to an elliptical shape to enhance its efficiency and overall performance. The system minimizes mechanical losses, thereby improving efficiency. Experimental methods were employed to evaluate the turbine's performance at various wind speeds in a wind tunnel under no-load and loaded conditions. A 5-watt/VAC Led lamp was used as the load, connected through a joule thief circuit with a DC input voltage ranging from 1.5 to 12 volts. The results indicate that incorporating an end plate—a component attached to the turbine rotor—allows the elliptical Savonius turbine to function effectively as an axial generator rotor. Voltage measurements showed that at wind speeds of 4 to 12 m/s, the turbine produced voltages ranging from 1.59 to 9.58 volts under no-load conditions. When loaded, the average voltage supplied was 2.26 volts, with a load current of 0.44A. This study demonstrates that the elliptical Savonius turbine integrated with an axial generator without gear transmission is a promising, low-cost solution for generating electrical energy from wind, offering both high efficiency and economic benefits.

1. INTRODUCTION

Renewable energy has been a major focus around the world as people become more concerned about climate change and the scarcity of fossil fuels [1]. Wind energy is one of the most promising renewable sources [2, 3]. Wind turbines can transform wind energy into electrical energy, and many types of turbines have been designed to maximize wind energy utilization. One interesting type of wind turbine is the Savonius turbine [4, 5]. The Savonius turbine, a slow-rotating wind turbine with two half-cylinder rotors connected by a central shaft, is not only simple but also remarkably durable. It can function in low wind conditions [6]. However, the classic Savonius turbine's efficiency is compromised by its variable torque, which reaches its maximum at specific rotor angles. Several review studies have been conducted on the Savonius turbine, mainly focusing on geometric design parameters [7-10], twisted bladed [11, 12], multiple quarter blades [13] various blade shapes [14], and number of blades [15-22]. Kurniawan et al. [23] modified the traditional Savonius turbine by adding multiple layers to the blade tips with an overlap ratio (OR) of 10 and 15%, respectively. The results revealed that the inclusion of numerous layers enhanced the power coefficient (Cp) by 22.4% and 11.2%.

Furthermore, the efficiency of elliptical Savonius turbines, as demonstrated by several researchers [24-27], is truly impressive. These turbines offer a range of advantages over conventional Savonius turbines, including a wider angle of attack, higher starting torque, lower tensile strength, and simplicity of design [28]. Their more streamlined shape allows for a more constant torque production. Numerous studies have looked into the lower torque ratio of classical turbines compared to elliptical turbines [29-31]. Kurniati et al. [32] also discovered that typical elliptical turbines are acceptable for usage in places with low wind speeds, demonstrating their efficiency.

Traditional Savonius turbines, on the other hand, have a higher CP capability at wind speeds l more significant than 10 m/s, indicating that they can be deployed and function better in areas with medium to high wind speeds. In addition, elliptical Savonius turbines have better rotational stability [33], meaning they are less prone to sudden changes in wind direction or speed, which can lead to more consistent energy production. These advantages make the elliptical-blade Savonius turbine an attractive option for a variety of renewable energy applications. This turbine has two half-cylinder rotors that rotate in opposite directions. The wind flowing around the rotors produces a torque that can be used to turn a generator and produce electricity.

In the energy conversion system, the DC generator is designed to have a higher generator voltage (V_G) than the load voltage (V_L). The generator must be rotated at that speed to attain the nominal voltage. When the generator does not rotate at the nominal speed, the output voltage is lower than the load voltage ($V_G<V_{Gnom}$). When $V_G \leq V_{Gnom}$, no power is transferred from the generator to the load, resulting in no energy conversion. One way to overcome this problem is to increase the generator rotor rotation by utilizing the energy transfer of gears coupled to the generator shaft and rotor. Several energy transfer techniques, such as pulleys, gearboxes, belts, and V

transmissions, are used to increase rotation. However, using a transmission system like this causes mechanical losses, requires maintenance, and equipment costs are quite expensive and cause noise [34]. In addition, using this transmission reduces the efficiency of the wind power plants (WPP) [35, 36]. Therefore, developing more efficient and environmentally friendly energy transfer technology, such as using a direct drive system or magnetic technology, is increasingly in demand to increase the efficiency of WPP. In addition, the use of this technology can also reduce maintenance costs and reduce noise generated.

Meanwhile, one turbine component (end plate) can be utilized for axial rotors by installing NdFeB magnetic teeth for axial generators without gear transmission. Integrating axial generators with this elliptical Savonius turbine will produce an innovative design that can increase the efficiency of wind energy used to generate electricity. Thus, using magnetic technology in WPP can provide dual benefits in terms of efficiency and operational costs. This proves that innovation in wind turbine design can positively contribute to renewable energy development.

On the other hand, in the study [37], an axial generator was designed for WPP needs. This study obtained the generator output voltage of 12-24 Volts with a rotation of 350-600 Rpm. With a unique design, this turbine can generate electricity without needing gear transmissions that require more intensive care and maintenance. The application of axial generators can be integrated directly with wind turbines without the need for additional complicated components to increase the efficiency and reliability of the wind power generation system. This integration will eliminate heat and friction losses usually occurring in conventional systems, thereby increasing energy efficiency. Using axial generators also allows wind turbines to operate at low speeds, generating electricity even when the wind blows slowly. In addition, this generator does not require lubrication, making it easier to maintain and ensuring its long-term viability. Integrating the Savonius turbine with an axial generator without gear transmission is expected to increase its efficiency and make it more economical for various applications.

This paper aims to develop the design of an elliptical Savonius turbine integrated with a gearless axial generator. The results of this experiment are expected to demonstrate that combining a Savonius turbine with a gearless axial generator can significantly enhance the efficiency and reliability of a wind power generation system. This integration will create opportunities for the development of more efficient and environmentally friendly renewable energy technologies.

2. MATERIALS AND METHODS

2.1 NdFeB coin magnet

NdFeB offers superior magnetic torque compared to other permanent magnets such as ferrite, AlNiCo, and Sm−Co. This magnet type contains the most energy of any permanent magnet. NdFeB magnets are the most common form of rare earth magnet due to their high magnetic strength relative to their physical size. Their coin-like or disc-like shape makes them suitable for a variety of applications. Their composition and structure consist of (1) neodymium (Nd), a rare earth element that provides strong magnetic properties; (2) iron (Fe), which contributes to magnetic strength; (3) boron (B), which plays an important role in the formation of the crystal structure responsible for superior magnetic properties; (4) tetragonal crystal structure which is the key to the strength of neodymium magnets [38].

NdFeB magnets, with their superior magnetic strength, are versatile and adaptable to a wide range of applications. Their remanence values range from 1.0 to 1.4 Tesla (T), and coercivity values (Hci) range from 750 to 2000 kA/m. The maximum energy product (BH_{max}) of NdFeB magnets ranges from 200 to 440 kJ/m^3, and they have a curie temperature (Tc) ranging from 310°C to 400°C. These properties make NdFeB coin magnets ideal for applications requiring limited space but significant magnetic strength. They are available in various diameters and thicknesses, allowing for adjustments to the needs of various applications, from everyday use to industrial and high-tech applications. In this study, coin magnets with a diameter of 25 mm and a thickness of 3 mm were used to manufacture generator rotor magnets (Figure 1).

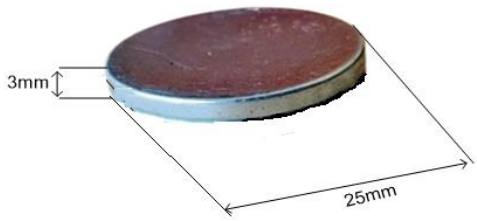

Figure 1. NdFeB coin magnet

2.2 Acrilyc material

Acrylic is a moisture-resistant, optically transparent thermoplastic with a high strength-to-weight ratio. Its lightweight nature, compared to metals like aluminum [39, 40], can significantly reduce the load on the turbine shaft, simplify assembly, and lessen the burden on the supporting structure. Acrylic's ease of cutting and shaping, using various methods, allows for the creation of endplates with intricate designs. With its excellent resistance to weather and ultraviolet (UV) light, it can withstand extreme conditions, providing reassurance in outdoor applications. Moreover, its impact resistance, which is about 17 times stronger than glass [41], makes it a safer and less prone to shattering material. According to Jung et al. [42], when a constant load of 1 kN is applied, increasing the exposure time to UV radiation initially leads to an increase in the mechanical properties of the acrylic material, followed by a gradual decrease. In contrast, when tests are conducted with a higher load of 3 kN, the material's mechanical properties show a significant increase with longer exposure times.

(a) (b)

Figure 2. Acrylic discs: (a) End-plate of turbine or rotor disc; (b) Stator disc

In this paper, we specifically address the materials used for the second plate of the elliptical turbine and the stator winding installation place of the axial generator. Particularly, we focus on the stator plate where the winding is positioned (Figure 2a) and the turbine end plate or bottom plate (Figure 2b) as a site for the coin magnet installation, each component being discussed in detail.

2.3 Testing procedure

The experimental setup, designed with meticulous attention to detail, is illustrated in Figure 3. The main components of a subsonic wind tunnel consist of five parts:

1) Settling chamber: Also known as a calming chamber, this section reduces turbulence in the airflow. It contains components such as a hanger and a screen.

2) Diffuser: This wind tunnel part features a gradually widening cross-sectional area. The diffuser increases air pressure as the air passes through it. According to Bernoulli's Principle, when fluid speed increases, pressure decreases, and vice versa. Therefore, as air moves through the diffuser, its speed decreases while its pressure increases.

3) Contraction section: This area has a gradually narrowing cross-section, serving the opposite function of the diffuser by increasing fluid velocity and decreasing pressure.

4) Test section: This is the wind tunnel area where the model or object to be tested is placed.

5) Fan: The fan generates airflow by creating suction or wind thrust. It is powered by a ½ HP AC motor and is equipped with a ventilation cover to control the wind speed. Overall, the wind tunnel has dimensions of 2.42 m × 1.11 m × 0.61 m.

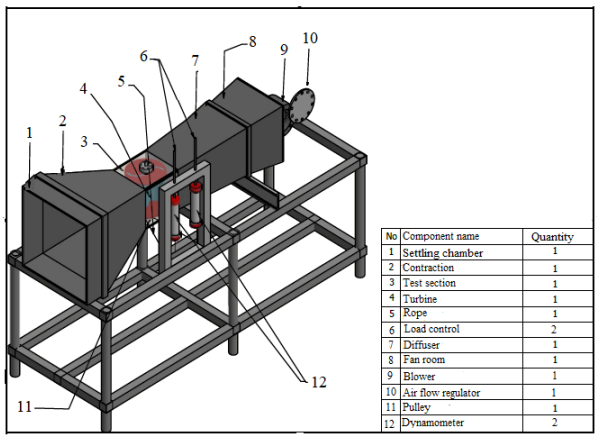

No	Component name	Quantity
1	Settling chamber	1
2	Contraction	1
3	Test section	1
4	Turbine	1
5	Rope	1
6	Load control	2
7	Diffuser	1
8	Fan room	1
9	Blower	1
10	Air flow regulator	1
11	Pulley	1
12	Dynamometer	2

(a)

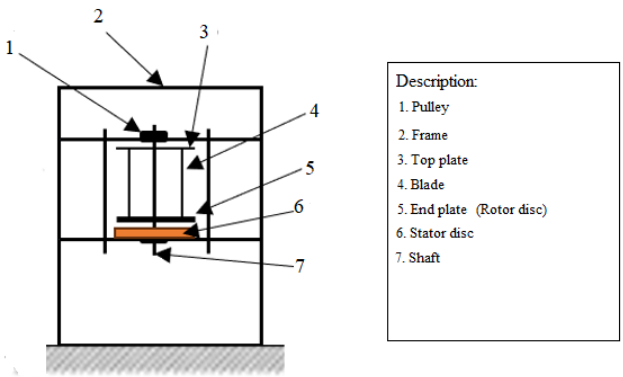

(b)

Figure 3. Experimental set up: (a) Schematic of the testing; (b) Photograph of the test rig

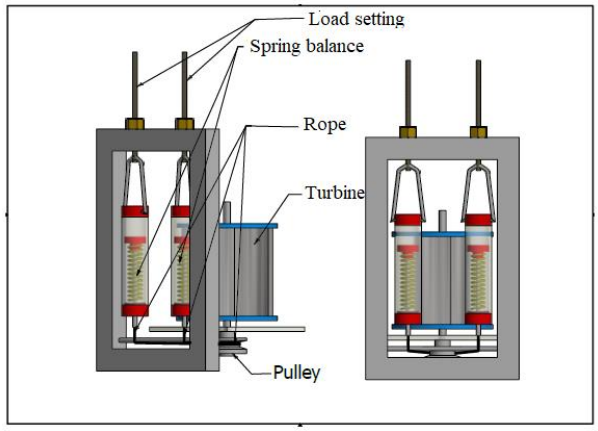

(a)

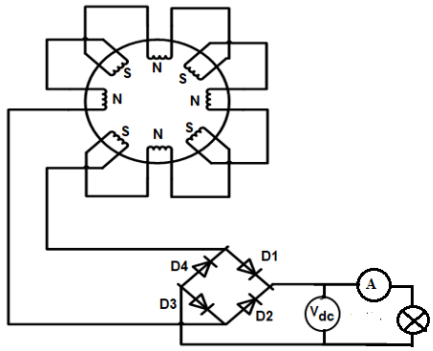

(b)

Figure 4. Test scheme: (a) Turbine force measurement (mechanical power / input power); (b) Electrical power measurement (output power)

In addition, the elliptical Savonius turbine prototype is equipped with NdFeB coin magnets mounted on the turbine end plate with eight poles and a stator disc with eight stator windings.

In this study, we conducted two tests: the mechanical system test, which measures the input power (Figure 4a), and the electrical system test, which measures the output power (Figure 4b). The mechanical system was assessed using a dynamometer to determine the turbine torque. The connection between power and torque in a turbine is illustrated in Figure 5.

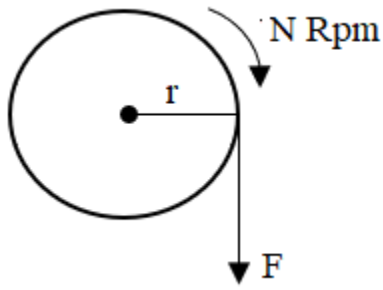

Figure 5. Pulley

Consider a pulley of radius r meter acting upon a circumferential force F Newton which makes it rotating at N Rpm. According to the definition of torque.

$$\tau = F \times r \text{ (N-m)} \qquad \text{(mechanical)} \qquad (1)$$

Work done per revolution = Force × distance = F × 2πr Joule
Power developed:

$$P = F \times 2\pi r\, N \quad \text{(Watt)} \\ = (F \times r) \times (2\pi N) = \tau \times \omega \quad \text{(Watt)} \tag{2}$$

where,
τ = Torque (N-m);
F = Driving force (N);
r = Radius (m);
ω = Angular velocity or 2πf N / 60 (Rad/s);
N = Rotational speed (Rpm);
P = Power (W).
Next, the electrical system applies:

$$P = V \times I \quad \text{(Watt)} \qquad \text{(Electrical)} \tag{3}$$

where,
P = Power (Watt);
I = Current (Ampere).
To calculate efficiency, Eq. (4) is used:

$$n = \frac{P_{out}}{P_{in}} \times 100\% \tag{4}$$

where,
P_{out} = Output power (Electrical power);
P_{in} = Input power (Mechanical power).
Therefore, several precision instruments have been integrated into the setup to ensure accurate measurements, including a Voltmeter, Anemometer, Dynamometer, and Tachometer. Before the experiment, the Savonius turbine and axial generator are installed in the wind tunnel's test section. The tests are performed with wind speeds ranging from 4 to 12 m/s. A Tachometer is used to measure the turbine's rotation, while an Anemometer measures the wind speed. The DC generator's output voltage is measured through the diode rectifier (bridge) attached to the end of the stator winding, and a DC Voltmeter is used to examine fluctuations in output voltage when wind speed changes.

2.4 Calculating the number of turns

The first step is to calculate the maximum magnetic flux using Eq. (5).

$$B_{max} = B_r \frac{l_m}{l_{m+\delta}} \tag{5}$$

where,
B_r = flux density, T;
δ = air gap width, m;
L_m = magnet diameter, m;
B_{max} = maximum magnetic flux, T.
For the magnetic area using Eq. (6).

$$A_m = \frac{\pi(r_0^2 - r_i^2 - rf(r_0 - r_i))N_p}{N_p} \tag{6}$$

where,
A_m = magnetic area, m^2;
r_o = outer radius of magnet, m;
r_i = inner radius of magnet, m;
N_p = number of poles;
rf = distance between magnets, m.
Then the maximum flux is obtained according to Eq. (7).

$$\emptyset_{max} = A_m \times B_{max} \tag{7}$$

where,
A_m = magnetic area, m^2;
$\emptyset_{max}$ = maximum flux, Wb.
Next, Eq. (8) is used to design the number of stators turns.

$$N = \frac{E}{4.44 \times f \times K_{w1} \times \Phi} \tag{8}$$

where,
N = number of turns;
E = phase voltage, volt;
f = frequency, Hz;
K_{w1} = winding factor (0.8);
ø = magnetic flux, Wb.
The winding factor (K_{w1}) is an important parameter that measures the efficiency of the stator winding in generating induced voltage compared to an ideal winding. Typically, the value of K_{w1} is less than 1 due to various factors, including the distribution factor (k_d) and the pitch factor (k_p) [43]. In simpler terms, the winding factor (K_{w1}) reflects the effectiveness of the stator winding in producing electromotive force (EMF) compared to an ideal winding setup. The distribution factor (k_d) suggests that the stator winding is not entirely concentrated in a single slot but is spread across multiple slots. This distribution reduces the induced EMF compared to a concentrated winding configuration. On the other hand, the pitch factor (k_p) indicates that the winding often does not utilize the entire length of the magnetic pole. Instead, the winding is typically shorter than the entire pole length to minimize harmonics and enhance the efficiency of the generator or transformer. The implications of a winding factor of 0.8 are as follows: (1) It reduces the number of turns required, as the windings do not fully contribute to the generation of electromotive force (EMF); thus, the number of turns needs to be adjusted accordingly. (2) There is an impact on efficiency, as a winding factor of less than 1 indicates a slight decrease in the efficiency of converting electromagnetic energy.

3. RESULTS

3.1 Magnetic flux measurement

Magnetic flux measurements were carried out on each magnet arranged into eight poles using a Tesla meter. The measurement of magnetic flux was conducted three times. Based on the data presented in Table 1, the average magnetic flux measurements for the eight magnetic poles are as follows: 172.3 mT, 170.7 mT, 170.3 mT, 167.7 mT, 171.0 mT, 170.0 mT, 171.0 mT, and 173.3 mT. The average magnetic flux measurement for the eight magnetic poles is 170.8 mT, equivalent to 0.171 T, with a standard error of 1.3%. This average serves as the basis for designing the stator winding.

Table 1. NdFeB coin magnet measurements

Measurement to	Magnetic Flux (mT)							
	N (1)	S (2)	N (3)	S (4)	N (5)	S (6)	N (7)	S (8)
1	175	172	175	173	165	170	175	173
2	169	169	166	167	173	171	169	174
3	173	171	170	163	175	169	169	173
Σ	517	512	511	503	513	510	513	520
$\bar{x}$	172.3	170.7	170.3	167.7	171.0	170.0	171.0	173.3
$\Sigma\bar{x}$	170.8							
d	-1.54	0.13	0.46	3.13	-0.21	0.79	-0.21	-2.54
D	2.25							
Error	1.3%							

Note: Σ = Total amount; $\bar{x}$ = Average; $\Sigma\bar{x}$ = Average amount
d = Deviation ($d_1=x_1-\Sigma\bar{x}$; $d_2=x_2-\Sigma\bar{x}$; $d_3=x_3-\Sigma\bar{x}$;……$dn=xn-\Sigma\bar{x}$)
D = Average deviation ($D=|d1|+|d2|+|d3|\ldots|dn|n$)
% Error in measurement = $D/\bar{x}\times 100\%$

3.2 Design development

3.2.1 Elliptical Savonius turbine design

Figure 6b illustrates the design of an elliptical Savonius turbine. The working principle of this turbine is similar to that of a conventional Savonius turbine in general (Figure 6a), with the key difference lying in the blade's shape. When the wind blows, the concave blade experiences a greater thrust than the convex blade, leading to the production of torque and the rotation of the turbine shaft. An elliptical Savonius turbine blade has a smoother and more curved profile compared to the conventional half-cylinder shape.

This elliptical shape offers several advantages, including better interaction between the blade and the wind flow, potentially resulting in greater torque and higher efficiency than conventional shapes [32]. The smoother shape also reduces turbulence and noise generated during rotation. Furthermore, the more even pressure distribution on the elliptical blade reduces the structural load on the turbine, making it a highly efficient and reliable choice in renewable energy.

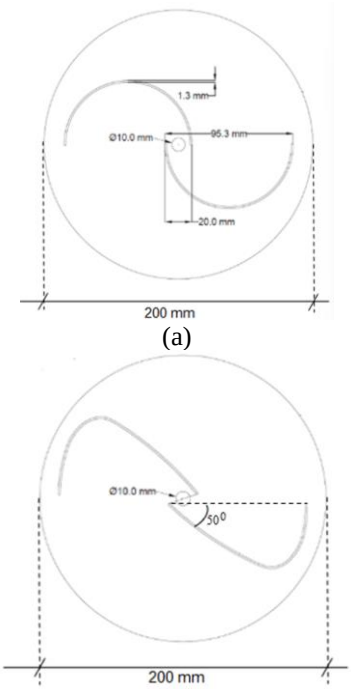

Figure 6. Savonius turbine design: (a) Conventional; (b) Elliptical

3.2.2 Axial generator design

A permanent magnet axial generator has a stator and rotor with a flux flow direction that cuts the stator axially (perpendicular). This generator produces alternating current (AC) electrical energy, as shown in Figure 7. One of the axial-type generators developed is the Axial Field Permanent Magnetic (AFPM), which is very well integrated with the Savonius turbine (Figure 7b). AFPM-type generators are gaining popularity due to their competitive pricing, particularly in high-energy permanent magnets.

This machine has various unique features or models and is extremely efficient since field excitation losses are minimized, resulting in significantly lower rotor losses [44]. This increases motor efficiency and allows for better power production [45]. Furthermore, AFPM is thinly thick and uses small magnets, resulting in compact generator dimensions and sizes [46]. AFPM can be built to take advantage of the increased power ratio coreless materials offer. Furthermore, AFPM's planar structure allows for easy air gap adjustment. Noise and vibration levels are lower than for typical machines (RFPM).

In this paper, we present a generator design that is both innovative and remarkably simple. The design features a single rotor, formed by utilizing the turbine end plate, which is circular in shape and houses a permanent magnet resembling a coin at its base. A stator disc, equipped with several wire coils, is also positioned at the end plate's base. An iron shaft is then installed between the rotor and stator, with both ends of the shaft connected to a pulley system, ensuring the smooth rotation of the rotor.

3.2.3 Proposed design

Figure 8 shows the design of an elliptical-type Savonius turbine integrated with an axial generator proposed in this study. Based on the engineering of the integration of the axial generator to the elliptical-type Savonius turbine, the main objective of this study is to develop an elliptical-type Savonius turbine topology by utilizing the turbine endplate as a generator rotor and adding one stator disc at the bottom of the turbine endplate. The number of stators turns installed in the stator disc groove is calculated based on the magnitude of the rotor coin magnetic flux. The magnitude of the rotor coin magnetic flux is measured using a Tesla meter. The installation of the stator disc with the turbine endplate disc has a space, which is an air gap or energy gap (δ). Permeability (μ) describes the magnetic force line effect in this air gap. Permeability is an object's ability to pass through magnetic force lines [47].

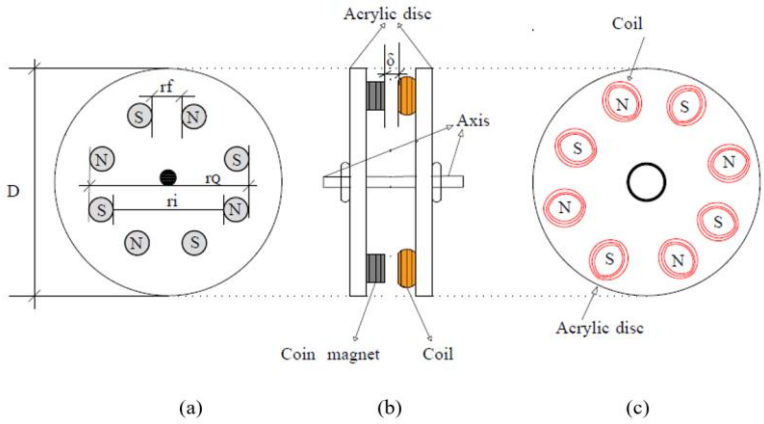

Figure 7. Axial generator design: (a) Rotor; (b) Rotor and Stator; (c) Stator

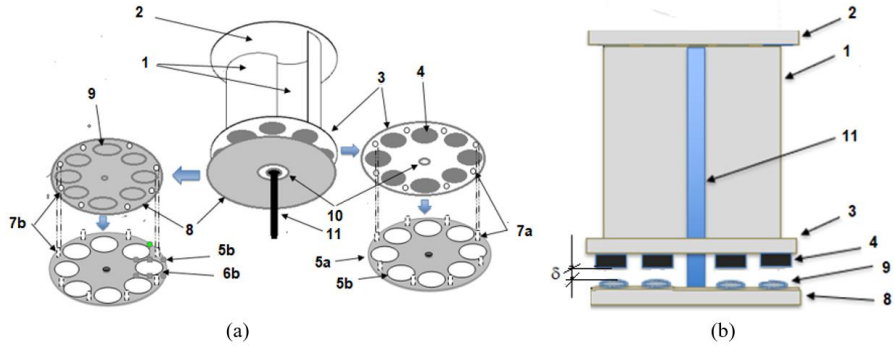

Note: 1. Elliptical type blade; 2. Top plate; 3. Endplate (Rotor plate); 4. Coin rotor magnet; 5. Rotor and stator plate cover (5a, 5b); 6. Rotor and stator plate groove (6a, 6b); 7. Bolts and nuts (7a, 7b); 8. Stator plate; 9. Stator winding; 10. Bearing; 11. Shaft.

Figure 8. Proposed design: (a) Design components; (b) Front view

The rotor designed in this study is made of a circular acrylic board with a diameter of 20 cm and a thickness of 8 mm. In this rotor section, the NdFeb coin magnet is installed on as many as eight poles, with a distance between magnets (rf) of 3.5 cm. Furthermore, the stator is a stationary part of the generator placed at the turbine endplate's bottom. The generator specifications can be seen in Table 2.

Table 2. Parameters of the integrated axial generator turbine studied

No.	Symbol	Parameter	Value
1	D	Disc diameter, (mm)	200
2	r_o	Magnet outer radius, (mm)	165
3	r_i	Magnet inner radius, (mm)	145
4	r_f	Distance between magnets (mm)	40
5	δ	Air gap distance, (mm)	10
6	l_m	Magnet diameter, (mm)	25
7	t_m	Magnet thickness, (mm)	3
8	B_r	Flux density, (T)	0.171
9	N_c	Number of coils	8
10	N_{ph}	Number of phases	1
11	N_p	Number of poles	8

3.3 Stator winding calculation

The calculation of the number of stator windings is done based on the total amount of rotor magnetic flux using Eqs. (5)-(8), as follows:

$$B_{max} = 0.171 \times \frac{0.25}{0.25 + 0.001} = 0.170 \text{ T}$$

Next, the magnetic area on the rotor is obtained:

$$A_m = \frac{3.14 \times (0.165^2 - 0.145^2) - 0.04 \times 8 \times (0.165 - 0.145)}{8} = 0.001633\ m^2$$

and,

$$\emptyset_{max} = 0.001633 \times 0.170 = 2.77 \times 10^{-4}$$

Then, planning a voltage of 12 Volts, we get:

$$N = \frac{12}{4.44 \times 50 \times 0.8 \times 2.77 \times 10^{-4}} = 243.93 \text{ turns (rounded to 250 turns)}$$

In this design, the stator is constructed using robust acrylic material, providing a sturdy base for the winding of coils arranged in series. Each of the eight wire coils is made from durable copper, with a diameter of 0.3 mm. In total, there are 250 turns in each coil, as shown in Figure 9.

Figure 9. Stator disc with a number of 8-pole windings

3.4 Experimental results

3.4.1 Wind speed and turbine rotation measurements

Turbine testing was carried out to assess the performance of the elliptical Savonius turbine at various wind speeds. The first test in this study was wind speed measurement, a process that was carried out with meticulous attention to detail. The wind speed measurement was conducted using an anemometer. When blown by the wind, the propellers on the anemometer will move according to the wind direction. The wind source in this test used a blower, causing the wind to flow in only one direction. The wind speed data obtained after measuring using an anemometer was 4-12 m/s. The subsequent measurement is the measurement of turbine rotation (Rpm) against wind speed variations. A Tachometer measuring an advanced instrument is used for the turbine rotation test. Before the measurement is carried out, a mark is given, for example, by giving a plain white sticker on the pulley surface to make it easier to determine the turbine rotation value (Rpm). The infrared or laser from the tachometer works by using a light sensor that is very sensitive to rotating elements. Figure 10 shows the results of wind speed and turbine rotation measurements without load. This measurement shows that at the lowest speed of 4 m/s, the turbine rotation is 57 Rpm, while at the highest wind speed, the turbine rotation is 546 Rpm.

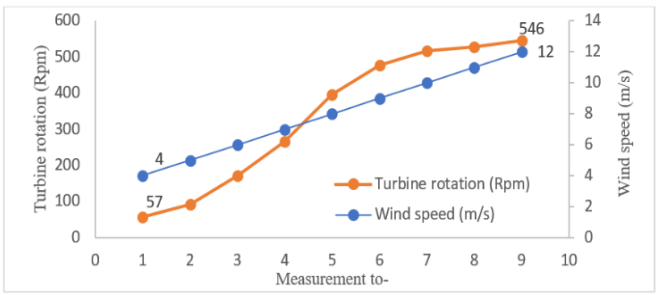

Figure 10. Wind speed measurement and turbine rotation without load

3.4.2 Output voltage measurement of axial generator

The primary purpose of output voltage measurement is to determine the magnitude of voltage produced by the generator at various operating conditions, such as at variations in rotor rotation speed. This information compares measurement results with theoretical values or calculated data. More importantly, it guides us in improving the generator design to produce a voltage that meets application needs. The output voltage measurement on axial generators is crucial in evaluating generator performance and obtaining data needed for design optimization. By conducting systematic measurements and analyzing the data obtained, we can understand the electrical characteristics of the generator and ensure that the generator operates as expected. Figure 11 shows the results of the output voltage vs. wind speed test. It can be seen that the highest output voltage is 9.80 volts at a wind speed of 12 m/s, while the lowest output voltage is 1.30 volts at a wind speed of 5 m/s. The output voltage consumed by the lamp load ranges from 2.24 to 2.27 volts. The average current consumed by the lamp load is 0.44 A. The changes in the light intensity vary. The light is bright at wind speeds of 7-12 m/s, while the wind speeds of 5-6 m/s (voltage below 1.41 volts).

Furthermore, Figure 12 illustrates the conditions of turbine rotation under both loaded and unloaded scenarios. When the turbine is loaded, its rotation speed decreases from 464.33 Rpm to 344.33 Rpm at a wind speed of 12 m/s. In the no-load condition, the lowest voltage output is recorded at 74 Rpm, which drops to 69 Rpm when the speed decreases to 5 m/s. This reduction in rotation speed is attributed to the low output current from the generator, which utilizes a wire diameter of only 0.3 mm.

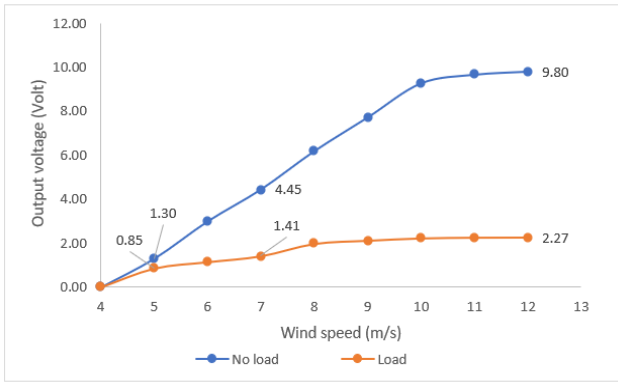

Figure 11. Measuring generator output voltage

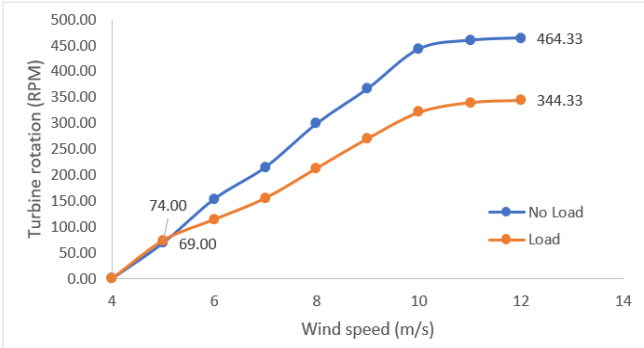

Figure 12. Measurement of turbine rotation ratio under no-load and loaded conditions

To maintain the stability of the generator's rotation when it is loaded, it is essential to consider both the amount of load and the nominal output current of the generator. Additionally, the lamp load employs a joule thief circuit, which operates at a DC voltage between 1.5 and 12 volts. The joule thief is a modified inverter circuit that converts direct current (DC) voltage to alternating current (AC) voltage [48, 49]. It is an electrical circuit that increases or amplifies the voltage by utilizing the operational principles of an inductor. This inductor, a passive electronic component, serves as a crucial energy conservation tool by storing energy in a magnetic field created by the electric current.

3.4.3 Efficiency analysis

The efficiency of a wind turbine is usually measured using the Cp, which indicates how much wind energy can be converted into electrical power. Theoretically, the maximum efficiency of a wind turbine is bound by the Betz Limit, which is approximately 59.3% of the total available wind kinetic energy [50].

Savonius turbines have lower efficiency than other turbines, with the Cp values ranging from 0.15 to 0.35 (15% to 35%). Several factors influence this efficiency, including wind speed,

the turbine's aspect ratio, and the turbine blades' design [4, 50]. This paper employs a modified elliptical blade design with an axis angle of 50°. According to Kurniati et al. [32], Savonius turbines modified with a 50°-axis angle demonstrate the highest Cp among elliptical blade modifications with 40°, 45°, and 55° axis modifications. However, these modified elliptical blades with a 50° angle cannot withstand wind speeds exceeding 9 m/s.

Additionally, the efficiency of a WPP is also influenced by the use of transmission systems such as belts and gearboxes. Theoretical efficiency for belt transmissions typically ranges from 90% to 98%, depending on the design and material used. In contrast, gearboxes tend to be more efficient, with efficiencies between 97% and 99%; however, they require lubrication and can be more costly to maintain.

In practical applications, the efficiency of both transmission types may be lower due to factors like friction, slippage, belt deformation, heat loss, and wear. The type of generator used also affects overall efficiency. Permanent magnet synchronous generators (PMSG) generally have an efficiency of 85% to 95%. In contrast, AFPM generators can achieve 95% to 98% efficiencies, as they benefit from shorter magnetic flux paths and reduced core losses. To calculate the total efficiency of the WPP system, refer to Eq. (9).

$$\eta_{total} = \eta_{turbin} \times \eta_{transmisi} \times \eta_{generator} \quad (9)$$

To compare efficiencies, let's assume the following: the efficiency of the Savonius turbine (Cp) is 30%, the efficiency of the belt transmission is 95%, and the efficiency of the PMSG is also 95%. In this scenario, the total efficiency of the system would be 27.01%. This means that only about 27.01% of the incoming wind energy is converted into electricity. In this innovation, the belt transmission is eliminated and replaced with an AFPM generator. As a result, we can expect an increase in overall efficiency:

$$\eta_{total} = \eta_{turbin} \times \eta_{AFPM\ generator} = 30 \times 98 = 29.4\% \text{ (there was an increase of about 2\%)} \quad (10)$$

Table 3 presents the results of mechanical power testing conducted at wind speeds ranging from 4 to 12 m/s. This data was collected through testing, as illustrated in the scheme shown in Figure 4(a). The data was then processed using Eqs. (1) and (2). Additionally, Table 4 displays the results of electrical power testing, which includes measurements of current and voltage. The output power was calculated using Eq. (3).

Furthermore, Figure 13 displays the wind energy conversion efficiency of the design proposed in this paper. The highest efficiency, measured at 28.83%, occurs at a wind speed of 9 m/s. However, as the speed increases to 10-12 m/s, the efficiency decreases due to the characteristics of the elliptical turbine modification, which has an axis angle of 50 degrees. This decrease is also affected by the small diameter of the stator coil, which measures only 0.3 mm.

According to Table 5, the current-carrying capacity of a 0.3 mm copper wire ranges from 0.141 to 0.212 A. Consequently, the current output from the axial generator remains relatively low. As a result, the 0.3 mm diameter wire can only conduct current within a limited range, and excessive heating occurs due to the wire's high resistance when the axial generator is loaded with 5 Watts. Suppose the current flowing through the wire exceeds it carrying capacity. In that case, significant I^2R power loss can occur, leading to decreased generator efficiency and the risk of damaging the wire due to overheating. Given these limitations, the generator struggles to handle larger loads effectively, which can cause a substantial drop in output voltage, as illustrated in Figure 10.

Table 3. Results of mechanical power measurements (input power) with varying wind conditions

Wind Speed (m/s)	Turbine Rotation (Rpm)	Angular Speed (ω)	Force 1 (F1)	Force 2 (F2)	Total Force (F2-F1)	Pulley Radius (r)	Torque (τ)	Mechanical Power (Pin)
4	50	5.23	0.1	0.3	0.2	0.1	0.02	0.52
5	78	8.16	0.1	0.2	0.1	0.1	0.01	0.82
6	114	11.93	0.1	0.3	0.2	0.1	0.02	1.19
7	150	15.70	0.1	0.4	0.3	0.1	0.03	1.57
8	200	20.93	0.2	0.6	0.4	0.1	0.04	2.09
9	267	27.95	0.2	0.7	0.5	0.1	0.05	2.79
10	328	34.33	0.3	0.8	0.5	0.1	0.05	3.43
11	340	35.59	0.3	0.9	0.6	0.1	0.06	3.56
12	344	36.01	0.4	1	0.6	0.1	0.06	3.60

Table 4. Results of testing current, voltage, and output power at varying wind speed conditions

Wind Speed (m/s)	Turbine Rotation (Average) (Rpm)	Output Voltage (Average) (Volts)	Output Current (Average) (Amps)	Power Output (Watts)	Light Conditions
4	0.00	0.00	0.00	0.000	Off
5	74.00	0.85	0.00	0.000	Off
6	114.33	1.14	0.00	0.005	Off
7	155.67	1.41	0.09	0.122	Off
8	213.33	1.97	0.16	0.309	Dim
9	270.67	2.12	0.38	0.806	On
10	321.00	2.23	0.44	0.980	On
11	340.00	2.26	0.44	0.994	On
12	344.33	2.27	0.44	0.997	On

Table 5. Copper wire diameter

Wire Diameter (mm)	Current Carrying Capacity (Ampere)
0.1	0.016 – 0.024
0.2	0.064 – 0.094
0.3	0.141 – 0.212
0.4	0.251 – 0.377
0.5	0.390 – 0.588
0.6	0.566 – 0.849
0.7	0.770 – 1.160
0.8	1.010 – 1.510
0.9	1.270 – 1.910
1.0	1.570 – 2.360
1.5	3.530 – 5.300
2.0	6.280 – 9.420

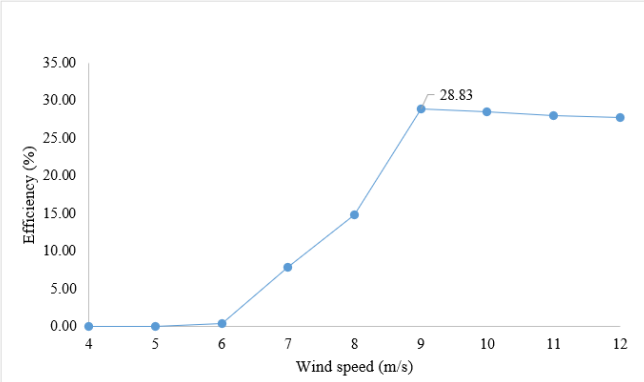

Figure 13. Energy conversion efficiency for wind speeds of 4-12 m/s

4. DISCUSSION

Experimental research on Savonius-type elliptical turbines with axial rotor generators without gear transmission is a field of study focused on developing small-scale energy. This technology offers a lightweight, compact, and easy-to-use energy source, especially in areas with high energy efficiency. Unlike using gear transmissions in wind power plants, this design produces friction and heat losses [51, 52]. The technology offered has higher efficiency and lower operating costs. In addition, this technology can provide smaller but effective turbines for energy generation, with the potential to significantly contribute to the global energy supply. Compared to gear or belt transmissions, this design can eliminate friction-related power losses, thereby increasing operational efficiency. In addition, the use of this technology also allows for a reduction in the size and weight of the turbine, making the installation and maintenance process more manageable.

Experimental studies of elliptical Savonius turbines with axial generators, a promising research area for future energy development, have shown their potential to provide a clean, cost-effective, and easily manufacturable source of electrical energy, especially in areas with low wind speeds. These turbines, which eliminate gear transmission, offer higher energy efficiency and operational reliability. The elimination of gear transmission significantly reduces energy losses due to friction and wear, ensuring these turbines' long-term reliability and durability.

The findings in this study are that the elliptical Savonius turbine with an axial generator without gear transmission can be a better choice for optimizing energy performance and durability. Thus, the development of this technology can make a positive contribution to the development of renewable energy in the future. Wind turbines can work more efficiently and last longer by eliminating friction and heat losses usually occurring in gear transmission. Technology without gear transmission can be a better solution for optimally producing electrical energy. In addition, the integration of this axial generator does not use an iron core. According to Leong et al. [53], a coreless AFPM generator has a smaller opposing EMF than a cored electric generator. The AFPM arrangement also offers zero cogging torque and a low starting torque. Eliminating ferrite material in the coreless electric generator will increase power generation.

Furthermore, the elliptical Savonius turbine, a key innovation in this study, offers a significant contrast to conventional designs. Its unique elliptical shape is designed to reduce drag and increase lift, particularly at specific wind angles, leading to higher torque and improved energy conversion efficiency. In contrast to conventional Savonius turbines, which often produce fluctuating torque, the elliptical shape is expected to mitigate this issue, resulting in smoother rotation and reduced system vibration. Thus, the elliptical form allows for more effective wind energy capture over a broader range of wind speeds, including low wind speeds.

In addition, as shown in Figure 12, there is a decrease in turbine speed under load conditions. This reduction in the speed of the axial generator occurs because the electromagnetic torque works against the aerodynamic torque generated by the wind. Although wind speed may increase, the rise in electrical load causes a larger current in the generator, which enhances the magnetic field's holding force. Consequently, the rotor speed remains lower than when operating under no-load conditions. This indicates that the balance between aerodynamic and electromagnetic torque largely determines the system's operating speed in a loaded wind turbine system. When the generator is subjected to an electrical load, an electric current flows through the stator winding. This current produces a magnetic field that opposes the rotor's main magnetic field, by Lenz's law. This creates an electromagnetic torque that counteracts the aerodynamic torque generated by the wind. In contrast, under no-load conditions (open circuit), the generator does not produce an electric current, resulting in minimal electromagnetic force (back EMF) to resist the rotor's movement. Under these conditions, the turbine rotor can rotate faster, as it only encounters relatively small aerodynamic resistance and mechanical friction.

5. CONCLUSIONS

Using elliptical shapes on Savonius turbine blades and their integration with gearless axial generators is an effective solution to increase the efficiency and performance of Savonius turbines. This innovation opens up new optimal wind energy utilisation opportunities, especially at low wind speeds. The use of gearless axial generators has several advantages:

1. Higher efficiency: Eliminating gears reduces energy losses due to mechanical friction, thereby increasing the efficiency of converting wind energy into electricity.

2. Easier maintenance: The absence of gears reduces mechanical complexity and maintenance requirements.

3. More compact design: directly integrating the turbine with the generator results in a more compact and lightweight

design.

4. Improved performance: Combining elliptical shapes on the blades and gearless axial generators results in improved overall Savonius turbine performance, especially at low wind speeds. This is important because most wind energy potential is at low wind speeds.

5. Potential applications: This innovation has the potential for small to medium-scale applications, such as wind power plants for households, offices, or remote areas.

6. Elliptical shape on turbine blades: Using an elliptical shape on Savonius turbine blades aims to optimize wind energy capture. This shape can reduce drag on blades that rotate against the wind and increase lift on blades that receive the wind, thus producing greater torque.

Some challenges and future research areas include:

1. Structure and material strength: The elliptical shape may require special considerations in material selection and structural design to ensure strength and resistance to wind loads.

2. Scale effects: The performance of the turbine and generator may vary depending on their size. Research is needed to understand the effect of scale on system efficiency and reliability.

3. Cost analysis: A comprehensive cost analysis is needed to evaluate the system's economic viability compared to other wind turbine technologies.

ACKNOWLEDGMENT

The author thanks the Ministry of Research, Technology, and Higher Education for funding this study under Research Contract No. 328/UN15.22/LT/2024.

REFERENCES

[1] Chen, H.M., Xu, Y.M. (2024). Industry energy dependence characteristics under different energy consumption accounting scopes: A comparison between China and the U.S. Sustainability, 16(22): 10121. https://doi.org/10.3390/su162210121

[2] Dewan, A., Gautam, A., Goyal, R. (2021). Savonius wind turbines: A review of recent advances in design and performance enhancements. Materials Today: Proceedings, 47(11): 2976-2983. https://doi.org/10.1016/j.matpr.2021.05.205

[3] Prasad, R.D., Bansal, R.C., Sauturaga, M. (2009). Wind energy analysis for vadravadra site in Fiji Islands: A case study. IEEE Transactions on Energy Conversion, 24(3): 750-757. https://doi.org/10.1109/TEC.2009.2025326

[4] Zemamou, M., Aggour, M., Toumi, A. (2017). Review of Savonius wind turbine design and performance. Energy Procedia, 141: 383-388. https://doi.org/10.1016/j.egypro.2017.11.047

[5] Karwa, N. Barve, S.B. (2021). Design, modelling and analysis of Savonius vertical axis wind turbine. International Research Journal of Engineering and Technology 8(11): 351-357.

[6] Laws, P., Saini, J.S., Kumar, A., Mitra, S. (2020). Improvement in Savonius wind turbines efficiency by modification of blade designs—A numerical study. Journal of Energy Resources Technology, 142(6): 061303. https://doi.org/10.1115/1.4045476

[7] Ramarajan, J., Jayavel, S. (2020). Numerical study of the effect of geometry and operating parameters on the performance of Savonius vertical axis wind turbine. Current Science, 119(12): 1927-1938.

[8] Worasinchai, S., Suwannakij, K. (2018). Performance characteristics of the Savonius turbine. IOP Conference Series: Materials Science and Engineering, 297: 012056. https://doi.org/10.1088/1757-899X/297/1/012056

[9] Chang, T.L., Tsai, S.F., Chen, C.L. (2021). Optimal design of novel blade profile for Savonius wind turbines. Energies, 14(12): 3484. https://doi.org/10.3390/en14123484

[10] Xisto, C.M., Páscoa, J.C., Trancossi, M. (2016). Geometrical parameters influencing the aerodynamic efficiency of a small-scale self-pitch high-solidity VAWT. Journal of Solar Energy Engineering, 138(3): 031006. https://doi.org/10.1115/1.4032794

[11] Saad, A.S., El-Sharkawy, I.I., Ookawara, S., Ahmed, M. (2020). Performance enhancement of twisted-bladed Savonius vertical axis wind turbines. Energy Conversion and Management, 209: 112673. https://doi.org/10.1016/j.enconman.2020.112673

[12] Elmekawy, A.M.N., Saeed, H.A.H., Kassab, S.Z. (2021). Performance enhancement of Savonius wind turbine by blade shape and twisted angle modifications. Proceedings of the Institution of Mechanical Engineers, Part A: Journal of Power and Energy, 235(6): 1487-1500. https://doi.org/10.1177/0957650920987942

[13] Sharma, S., Sharma, R.K. (2016). Performance improvement of Savonius rotor using multiple quarter blades—A CFD investigation. Energy Conversion and Management, 127: 43-54. https://doi.org/10.1016/j.enconman.2016.08.087

[14] Hassan Saeed, H.A., Nagib Elmekawy, A.M., Kassab, S.Z. (2019). Numerical study of improving Savonius turbine power coefficient by various blade shapes. Alexandria Engineering Journal. 58(2): 429-441. https://doi.org/10.1016/j.aej.2019.03.005

[15] Wenehenubun, F., Saputra, A., Sutanto, H. (2015). An experimental study on the performance of Savonius wind turbines related with the number of blades. Energy Procedia, 68: 297-304. https://doi.org/10.1016/j.egypro.2015.03.259

[16] Hassanzadeh, R., Mohammadnejad, M., Mostafavi, S. (2021). Comparison of various blade profiles in a two-blade conventional Savonius wind turbine. Journal of Energy Resources Technology, 143(2): 021301. https://doi.org/10.1115/1.4047757

[17] Kumar, R.S., Premkumar, T.M., Seralathan, S., Xavier, D.D., Elumalai, E.S., Hariram, V., Sabapathi, S. (2020). Simulation studies on influence of shape and number of blades on the performance of vertical axis wind turbine. Materials Today: Proceedings, 33: 3616-3620. https://doi.org/10.1016/j.matpr.2020.05.665

[18] Zhao, T.Y., Zhang, X., Zheng, M.S. (2020) Blade number effect on the optimal energy efficiency for a modified Savonius rotor. Proceedings of Institution of Civil Engineers: Energy, 173(3): 101-108. https://doi.org/10.1680/jener.19.00031

[19] Prabowoputra, D.M., Prabowo, A.R., Hadi, J.M., Sohn, S. (2021). Assessment of turbine stages and blade numbers on modified 3D Savonius hydrokinetic turbine performance using CFD analysis. Multidiscipline Modeling in Materials and Structures, 17(1): 253-272.

https://doi.org/10.1108/MMMS-12-2019-0224
[20] Mansour, H., Afify, R. (2020). Design and 3D CFD static performance study of a two-blade icewind turbine. Energies, 13(20): 5356. https://doi.org/10.3390/en13205356
[21] Alhumimidi, S. M. (2020). An integrated approach for identification of seawater intrusion in coastal region: A case study of northwestern Saudi Arabia. Journal of King Saud University – Science, 32(7): 3187-3194. https://doi.org/10.1016/j.jksus.2020.09.010
[22] Jeeva, B., Sandeep, S.J., Ramsundram, N. (2019). Effect of blade number and angle on the characteristics of the Savonius type wind turbine. Journal of Physics: Conference Series, 1380: 012110. https://doi.org/10.1088/1742-6596/1380/1/012110
[23] Kurniawan, Y., Dwi Prija Tjahjana, D.D., Santoso, B. (2020). Experimental study of Savonius wind turbine performance with blade layer addition. Journal of Advanced Research in Fluid Mechanics and Thermal Sciences, 69(1): 23-33, https://doi.org/10.37934/ARFMTS. 69.1.2333
[24] Dewan, A., Bishnoi, A.K., Singh, T.P., Tomar, S.S. (2023). Elliptical bladed Savonius rotor for wind energy: Efficacy of RANS modeling for flow characteristics. Journal of Energy Resources Technology, 145(5): 051301. https://doi.org/10.1115/1.4056275
[25] Alom, N., Kolaparthi, S.C., Gadde, S.C., Saha, U.K. (2016). Aerodynamic design optimization of elliptical-bladed Savonius-style wind turbine by numerical simulations. In ASME 2016 35th International Conference on Ocean, Offshore and Arctic Engineering, Busan, South Korea, pp. 1-7. https://doi.org/10.1115/OMAE2016-55095
[26] Alom, N., Saha, U.K. (2017). Arriving at the optimum overlap ratio for an elliptical-bladed Savonius rotor. In ASME Turbo Expo 2017: Turbomachinery Technical Conference and Exposition, Charlotte, North Carolina, USA, pp. 1-10. https://doi.org/10.1115/GT2017-64137
[27] Kaya, A.F., Acir, A., Kaya, E. (2023). Numerical investigation of wind-lens combinations for improving aerodynamic performance of an elliptical-bladed Savonius wind turbine. Journal of the Brazilian Society of Mechanical Sciences and Engineering, 45: 309. https://doi.org/10.1007/s40430-023-04216-8
[28] Banerjee, A. (2019). Performance and flow analysis of an elliptic bladed Savonius-style wind turbine. Journal of Renewable and Sustainable Energy, 11: 033307. https://doi.org/10.1063/1.5097571
[29] Banerjee, A., Sukanta, R., Mukherjee, P., Saha, U.K. (2014). Unsteady flow analysis around an elliptic-bladed Savonius-style wind turbine. In ASME 2014 Gas Turbine India Conference, New Delhi, India, pp. 1-7. https://doi.org/10.1115/gtindia2014-8141
[30] Kacprzak, K., Liskiewicz, G., Sobczak, K. (2013). Numerical investigation of conventional and modified Savonius wind turbines. Renewable Energy, 60: 578-585. https://doi.org/10.1016/j.renene.2013.06.009
[31] Talukdar, P.K., Kulkarni, V., Saha, U.K. (2021). Aerodynamic performance characterization of a drag-based elliptical-bladed Savonius wind turbine rotor. Gas Turbine India Conference, 85536: V001T09A005. https://doi.org/10.1115/GTINDIA2021-76001
[32] Kurniati, S., Syam, S., Sanusi, A. (2023). Numerical investigation and improvement of the aerodynamic performance of a modified elliptical-bladed Savonius-style wind turbine. AIMS Energy, 11(6): 1211-1230. https://doi.org/10.3934/ENERGY.2023055
[33] Shende, V., Patidar, H., Baredar, P., Agrawal, M. (2022). A review on comparative study of Savonius wind turbine rotor performance parameters. Environmental Science and Pollution Research, 29: 69176-69196. https://doi.org/10.1007/s11356-022-22399-w
[34] Deshmukh, S., Bhattacharya, S., Jain, A., Paul, A.R. (2019). Wind turbine noise and its mitigation techniques: A review. Energy Procedia, 160: 633-640. https://doi.org/10.1016/j.egypro.2019.02.215
[35] Marques, P.M.T., Fernandes, C.M.C.G., Martins, R.C., Seabra, J.H.O. (2013). Power losses at low speed in a gearbox lubricated with wind turbine gear oils with special focus on churning losses. Tribology International, 62: 186-197. https://doi.org/10.1016/j.triboint.2013.02.026
[36] Michaelis, K., Höhn, B.R., Hinterstoißer, M. (2011). Influence factors on gearbox power loss. Industrial Lubrication and Tribology, 63(1): 46-55. https://doi.org/10.1108/00368791111101830
[37] Syam, S., Kurniati, S. (2022). Experimental study of the design of axial flux permanent magnet generator using layers of rectangular NdFeB magnet for small wind power applications. Journal of Engineering Science and Technology Review, 15(1): 177-184, https://doi.org/10.25103/jestr.151.22
[38] Lewis, L.H., Jiménez-Villacorta, F. (2013). Perspectives on permanent magnetic materials for energy conversion and power generation. Metallurgical and Materials Transactions A: Physical Metallurgy and Materials Science, 44(Suppl 1): 2-20. https://doi.org/10.1007/s11661-012-1278-2
[39] Candlin, J.P. (2008). Chapter 3 polymeric materials: Composition, uses and applications. Comprehensive Analytical Chemistry, 53: 65-119. https://doi.org/10.1016/S0166-526X(08)00403-0
[40] Kumar, A., Kumar, N. (2022). Advances in transparent polymer nanocomposites and their applications: A comprehensive review. Polymer-Plastics Technology and Materials, 61(9): 937-974. https://doi.org/10.1080/25740881.2022.2029892
[41] Oral, M.A. (2019). Production and characterization of polyester/poly (methyl methacrylate) and acrylonitrile butadiene stryrene terblends and nanocomposites. PhD thesis, İstanbul Technical University.
[42] Jung, D.Y., Abdel Hay, A., Lim, J.K. (2012). Study on applied load and irradiation of ultraviolet (UV) aging of polycarbonate characteristics: Consequences on mechanical properties. Advanced Materials Research, 472-475: 1361-1365. https://doi.org/10.4028/www.scientific.net/AMR.472-475.1361
[43] Chapman, S.J. (2012). Electric Machinery Fundamentals (Fifth edition). McGraw Hill Companies Inc.
[44] Aydin, M., Huang, S., Lipo, T.A. (2004). Axial flux permanent magnet disc machines: A review. Research Report 2004-10, pp. 61-71.
[45] Huang, S., Aydin, M., Lipo, T.A. (2001). Torque quality assessment and sizing optimization for surface mounted permanent magnet machines. In Conference Record of the 2001 IEEE Industry Applications Conference. 36th IAS Annual Meeting (Cat. No.01CH37248), Chicago,

IL, USA, pp. 1603-1610. https://doi.org/10.1109/IAS.2001.955749
[46] Cavagnino, A., Lazzari, M., Profumo, F., Tenconi, A. (2002). A comparison between the axial flux and the radial flux structures for PM synchronous motors. IEEE Transactions on Industry Applications, 38(6): 1517-1524. https://doi.org/10.1109/TIA.2002.805572
[47] Gao Q.Z., L.S., Wang D.Z., Lin, S. (2014). Application of field theory to air gap permanent magnet eddy current coupling. Advanced Science and Technology Letters, 73: 44-51. http://doi.org/10.14257/astl.2014.73.08
[48] Chopda, R.A., Gupta, Kabra, P., Dwivedi, P. (2021). Joule thief and its applications. International Journal for Research in Applied Science and Engineering Technology, 9(12): 31-34. https://doi.org/10.22214/ijraset.2021.39190
[49] Budisusila, E.N., Arifin, B. (2017). Joule-thief circuit performance for electricity energy saving of emergency lamps. IOP Conference Series: Materials Science and Engineering, 190(1): 012017. https://doi.org/10.1088/1757-899X/190/1/012017
[50] Ranjbar, M.H., Nasrazadani, S.A., Kia, H.Z., Gharali, K. (2019). Energy equipment and systems reaching the betz limit experimentally and numerically. Energy Equipment. Systems, 7(3): 271-278. https://doi.org/10.22059/EES.2019.36563
[51] Matsumura, S., Hamasaka, N. (2006). High strength and compactness of gears by WHSP (double hard shot peening) technology. Komatsu Technical Report, 52(158): 1-5. https://www.komatsu.jp/en/company/tech-innovation/report/pdf/158-03_E.pdf.
[52] Spanoudakis, P., Moschopoulos, G., Stefanoulis, T., Sarantinoudis, N., Papadokokolakis, E., Ioannou, I., Piperidis, S., Doitsidis, L. Tsourveloudis, N.C. (2020). Efficient gear ratio selection of a single-speed drivetrain for improved electric vehicle energy consumption. Sustainaibility, 12(21): 9254. https://doi.org/10.3390/su12219254
[53] Leong, Y.W., Razali, A.R., Priyandoko, G., Kasim, N. I. (2016). Preliminary studies on number of coil turns per phase and distance between the magnet pairs for AFPM ironless electricity generator. MATEC Web of Conferences, 38: 03003. https://doi.org/10.1051/matecconf/20163803003

NOMENCLATURE

AC	alternating current, Vac
AFPM	axial field permanent magnetic
A_m	magnetic area, m^2
B	boron
BH_{max}	maximum energy product
Br	flux density, T
Cp	power coefficient
DC	direct current, Vdc
E	phase voltage, volt
EMF	electromotive force
F	frequency, Hz
Fe	iron
Hci	coercivity values
kd	distribution factor (kd)
kp	pitch factor
Kw	winding factor
N	number of turns
NdFeB	neodymium iron boron
Np	number of poles
OR	overlap ratio
PMSG	permanent magnet synchronous generators
RFPM	radial flux permanent magnet
Rf	distance between magnets, m
r_i	inner radius of magnet, m
r_o	outer radius of magnet, m
Rpm	revolutions per minute
T	Tesla
Tc	curie temperature
UV	ultraviolet
VG	generator voltage
VL	load voltage
WPP	wind power plants

Greek symbols

δ	air gap disance, m
Φ	magnetic flux, Wb
Ø	magnetic flux, Wb
$Ø_{max}$	maximum flux, Wb
μ	permeability
ω	angular velocity